Donald B. Olson, Ge Peng, George R. Halliwell and Cristina Forbes

Evolution of Turbulence as a Function of Initial Flows on a Beta Plane

Abstract

The evolution of the wavenumber spectra and energy balances in turbulent channel flows on a beta plane is considered using a three-layer isopycnal model. The initial conditions for the experiments are selected from an analytical study of the stability of three-layer channel flows representative of various oceanic gyre regimes. Experiments are integrated for 400 days following initialization of the various flow states with superimposed white noise perturbations. In most of the states there is an initial adjustment period which follows the linear wave growth expected from the analytical computation. This is followed by a cascade to larger scales and a filling in of the wavenumber spectra. The onset of steady inertial ranges in the model spectra occurs as an event-like shift that occurs earlier in westward flows than it does in eastward currents. For stable or near neutral initial conditions the spectra only have a limited region that might be termed inertial. These stochastically forced turbulent states without additional energy input from the mean flows exhibit low PE spectral slopes, k^{-3} or less. The higher energy runs where the turbulence is dominated by energy input from baroclinic instability exhibit steeper PE spectra, $\sim k^{-5}$. Energetics of these states are also discussed along with comparisons with observed oceanic energetics and energy spectra based on satellite altimeters.

Introduction

Spectral closure theories for turbulence following Kolmogoroff (1941) have centred attention on various inertial ranges which arise depending on the controlling factors in the flow (*cf.* Vallis, 1992 for an up to date review of 2-D theories). Spectral theories for oceanic turbulence have made various predictions concerning the wavenumber structure expected (*cf.* Charney, 1971; Rhines, 1977; Salmon, 1982). Early attempts to verify these predictions were thwarted by sampling of dynamical variables that was inadequate to span the range of spatial scales required to resolve these inertial ranges (Dantzler, 1976). Observations that did resolve an adequate range of scales were made for "passive" variables such as sea surface colour or temperature (Denman and Platt, 1980; Gower *et al.*,

1980). One might also consider using mooring data in combination with Taylor's advection hypothesis to reconstruct wave number spectra. Again, the results would at least be suspect. The availability of sea level height measurements from satellite altimeters has changed this state of affairs by providing abundant spatial data (Fu, 1983; Le Traon *et al.*, 1990; Forbes *et al.*, 1993). A representative set of spectra averaged in 10° squares in the South Atlantic from Forbes *et al.* (1993) is shown in Fig. 1. There is a broad range of spectral slopes from k^{-2} in the quieter northeastern subtropical gyre to values with slopes near k^{-4} in the Agulhas and Brazil/Malvinas regions. Individual satellite tracklines in the Brazil and Agulhas have slopes of k^{-5} (not shown). Similar results in the North Atlantic are given in Fu (1983) and Le Traon *et al.* (1990). In the present study the goal is to explore the dynamics behind this range of spectral fall-offs. This will involve both characterizing and understanding the relationship between wavenumber spectra of surface height and kinetic energy (KE) since most turbulence closure theories predict the slope of KE spectra while altimeters sample the surface height (η) variability.

A starting place is Fu's (1983) analysis and its relationship to Charney (1971, 1973). Charney's analysis explicitly suggests that both KE and PE have a k^{-3}

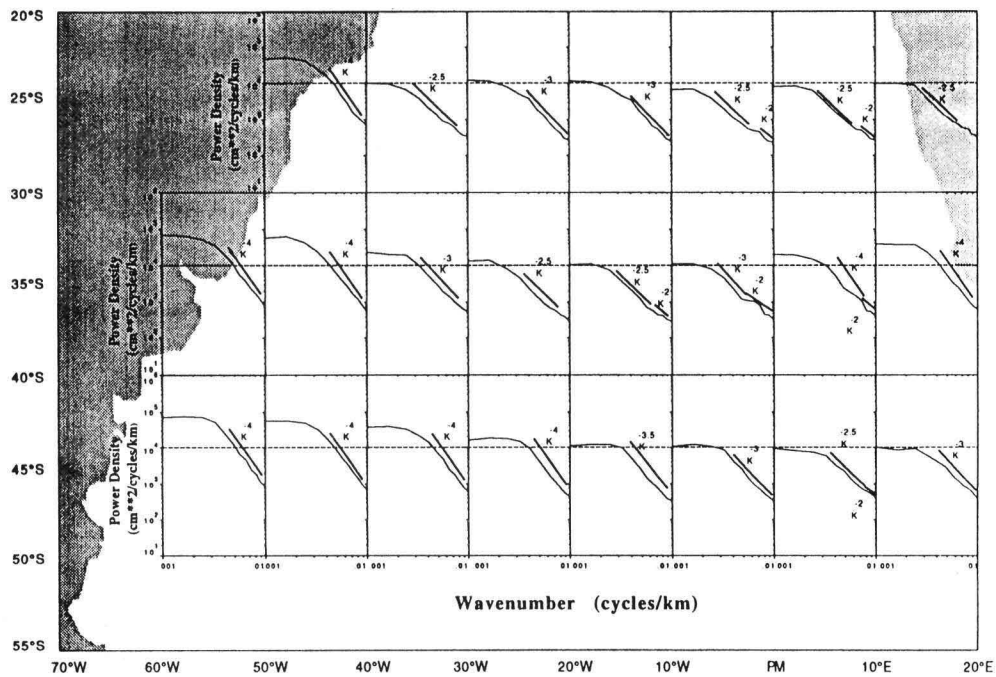

Fig. 1. Sea level height wavenumber spectra by ten degree square for the South Atlantic subtropical gyre from Forbes *et al.* (1993). Data are based on individual satellite trackline data spectra averaged over the squares shown. Altimeter sea surface height anomalies are from the GEOSAT mission. The dashed line through each spectrum indicates the 10^4 cm/(cycle km) energy level. Spectral slope lines are given for reference.

spectral dependence below the radius of deformation (R_D). This is concise within the bounds of quasi-geostrophic theory as demonstrated by Hua and Haidvogel (1986). In contrast, Fu's suggestion that the KE spectra should be k^{-2} times the PE spectra, *i.e.* $\eta^2 \sim k^{-5}$, is intuitively based on the geostrophic relation. More formally, if we assume that both PE and KE are locally transferred in wavenumber space in the inertial range and that the eddies are in near geostrophic balance, then PE $\propto \eta^2$ and KE $\propto k^{-2}\eta^2$ or η^2/L^2 at each eddy scale. Fu's scaling, PE $\sim k^{-2}$KE, is only consistent with Charney's assumption of equi-partition between KE and PE for $L \leqslant R_D$ near the radius of deformation. Charney's result is consistent with the quasi-geostrophic result that as $L \to R_d$, KE $\to$ PE. For this problem the appropriate scaling parameter to consider is the Burger number, $B = R_d^2/L^2$. Quasi-geostrophic theory predicts KE/PE $\propto B$ for baroclinic motions, exactly the relationship of Fu (1983). This relationship is borne out in observations of individual rings (Olson, 1991). This scaling requires extension theoretically into more nonlinear parameter domains as suggested by Cushman-Roisin *et al.* (1992) and Tang and Cushman-Roisin (1992) and observationally to a larger range of oceanic eddies.

Theories for spectral slopes associated with different inertial ranges arise from assumptions made about the dynamical controls on turbulent cascades. The k^{-3} solution follows from the assumption that it is enstrophy dissipation that is the controlling factor (Kraichnan, 1967; Salmon, 1982). Charney's (1971) contribution is the extension of this to geophysical flows. An assumption that there is a separate range controlled by an energy flux to larger scales leads to a $k^{-5/3}$ spectrum (Salmon, 1982) which is analogous to the three dimensional turbulence result of Kolmogoroff (1941). Various other inertial ranges have been hypothesized. Rhines (1975), for example, suggests k^{-5} based on a similarity theory for turbulence on a β-plane. His treatment assumes the relevant similarity variables are the wave number and the short Rossby wave group velocity, $E = E(k, C_g)$; $C_g = \beta/2k^2$. Accepting the Rhines (1975) formulation for the kinetic energy spectra and applying the quasi-geostrophic scaling gives a k^{-7} spectra for PE. Of course, there is nothing in the Rhines case that distinguishes between PE and KE. One could assume that the similarity holds in PE and therefore PE $\sim k^{-5}$ and KE $\sim k^{-3}$. A full range of Rossby waves in spectral space would have variable KE/PE ratios under the arguments above and are expected to have dispersive dynamics. Note that an ambiguity in whether KE or PE scales to the similarity variables does not appear in the case of the k^{-3} arguments for two or quasi-two dimensional flows described in the previous paragraph. Those results are based on enstrophy arguments and therefore can be directly tied to the KE spectra. Another alternative, within the rules of the similarity arguments, would be to invoke β without any assumption of Rossby wave dynamics. Following the arguments of Nof (1981) concerning the planetary induced motion in coherent vortices, if $E = E(k, \beta)$ then by similarity $E \sim k^{-4}$. Finally as pointed out by Fu (1983), the existence of fronts must be considered. Andrews and Hoskin (1978) obtain $k^{-8/3}$ for inertial ranges in flows involving significant frontogenesis. A view of fronts as steps or "edges" in

property distributions will alternatively produce k^{-2} spectral slopes through Gibb's phenomenon (Phillips, 1971).

The wealth of different potential rationale for the spectral fall off and the altimeter observations of a range of spectral slopes in various portions of subtropical gyres (Fig. 1) suggest a division of the gyre into different dynamical regimes. These different regimes may reflect changes in the manner in which the turbulent field is forced (Hua and Haidvogel, 1986; Le Traon *et al.*, 1990). The changes across the gyre may reflect the differences between eddy fields which arise from instability of the mean flow versus areas where the eddy field is derived directly from wind forcing (Le Traon *et al.*, 1990). Here a set of numerical simulations exploring the linear stability space for various flow conditions found in ocean gyres will be explored to test the conjecture that flows forced to turbulence via local instability have higher spectral fall-off rates than flows forced either by random winds (Le Traon *et al.*, 1990), or in the present case by random initial perturbation fields superimposed on a flow.

Choice of models

The basic choice of models is meant to provide a fairly complete set of ocean-like flows while retaining some analytic capability. The analytic calculations allow the stability of various flow regimes to be addressed. These are then used to specify initial conditions for primitive equation simulations. Both computations consider a three layer isopycnic, periodic channel model with unequal layer mean thicknesses and reduced gravities typical of subtropical gyre circulations. These give radii of deformation of 30 km for the upper layer and 46 km for the second layer. The analytic solutions are from a linearized, quasi-geostrophic case (Halliwell *et al.* 1994) with the same model geometry. The linear formulation follows the development of Davey (1977, see also Pedlosky, 1979) except in the choice of unequal layer thickness. The model configuration is the minimum needed to capture the various shears across the upper interface representing the upper thermocline and the lower isopycnal surface representing the deep main thermocline. The stability space along with schematics of the isopycnal (interface) geometries for the four quadrants of the space are shown in Fig. 2. The various letters on the diagrams in Fig. 2 indicate the numerical simulations completed using the isopycnal model of Bleck and Boudra (1986) and Boudra *et al.* (1988). The numerical model is a primitive equation formulation with Lagrangian vertical coordinates. Here it is used in a zonally-periodic β-plane channel geometry, 20 km grid, and Laplacian viscosity ($K_H = 100\ m^2/s$).

The simulations are initialized with a given interface profile and then perturbed with a deformation process which sharpens the flow in the central channel (Boudra *et al.*, 1988; Halliwell *et al.*, 1994). This is followed by the addition of white noise perturbations to the meridional velocity field. The points in the stability space (Fig. 2.) are based on zonal average conditions following the deformation step. Following the initial deformation step and the addition of the

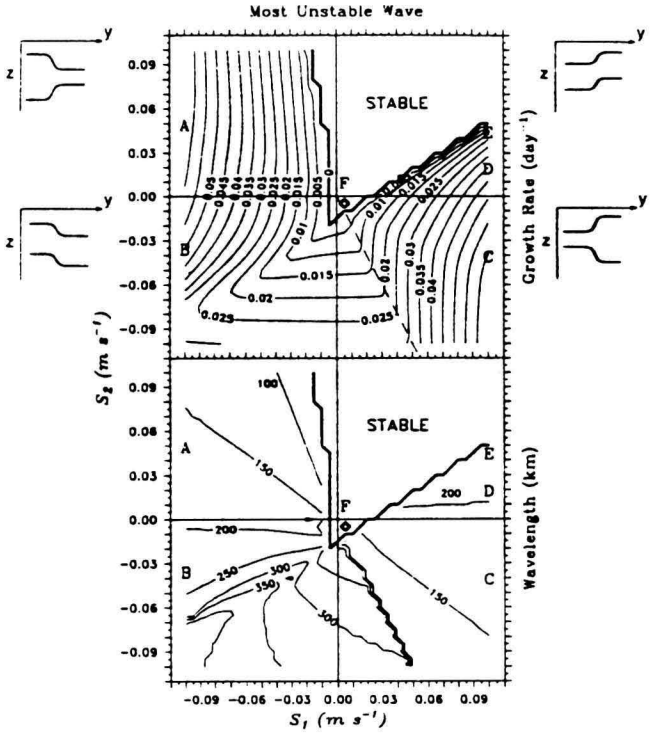

Fig. 2. The linear stability space for the initial conditions used in the numerical simulations. The axes indicate the shear in zonal velocity across the upper (S1) and lower (S2) interfaces. The geometry of the interface slopes for these cases are shown to the side of each quadrant in the upper diagram with contours of linear unstable wave growth rate. The lower panel shows the wavelength of maximum growth rate. The letters on the diagrams show the shears relevant for the model runs. The basic geometry of the two pycnoclines in each quadrant of the diagrams is shown schematically with the upper figure (y positive northwards). Full discussion of the linear model and its application to conditions in subtropical frontal zones (case C) can be found in Halliwell *et al.* (1994).

white noise perturbations, the simulations are no longer forced. In this sense these are spin-down experiments and can never reach a formal equilibrium state. The model simulations are integrated out to 411 days in each case. Further elaboration of both the analytic and numerical models can be found in the discussion of a set of experiments representing the subtropical convergence frontal zone in the Atlantic (Fig. 2, point C) which is the essential objective of the Halliwell *et al.* (1994) study.

Spectral evolution and energetics

While each point in the stability regime evolves differently, overall the behaviour can be broken down into points that fall in the stable or near neutral domain (E,F) and those that are unstable (A,B,C,D). The final spectra of the sea surface

height as diagnosed in the model at 411 days for each of the six points in Fig. 2 are shown in Fig. 3a. The neutral and stable conditions produce spectral peaks associated with the resonance in the channel and an underlying slope of k^{-2} in η (Fig. 3a). This would suggest under Fu's (1983) hypothesis that the kinetic energy spectrum is close to the initial perturbation spectrum and essentially white. The model, however, produces a very steep KE spectrum with slopes between -5 and -6 (Fig. 3b). For the unstable cases all of the η spectra approach $\sim k^{-5}$ in

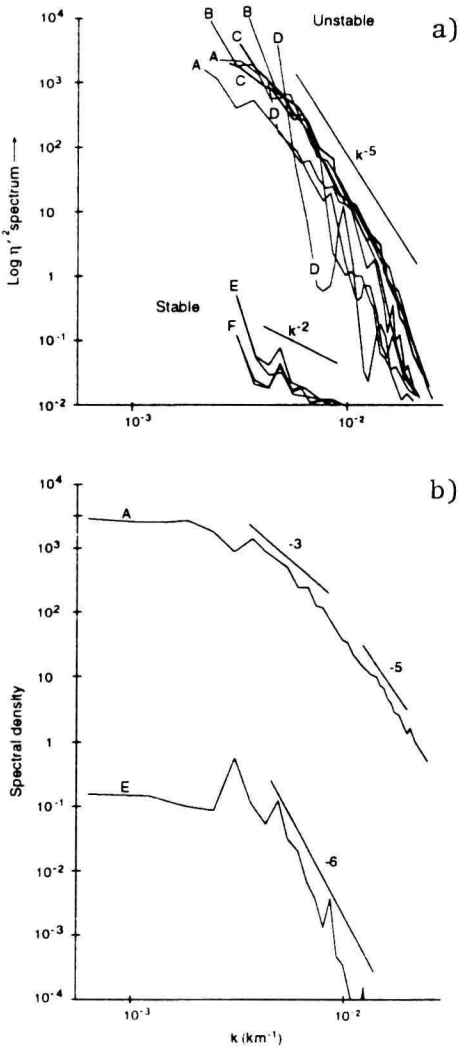

Fig. 3. a) End state surface height spectra for the various model runs for the stability space shown in Fig. 2. Data are for the last portion of each of the runs when the spectra are nearly at equilibrium (200-400 days). Two spectra approximately 100 days apart are shown for each case. b) Kinetic energy spectra on day 411 for cases A and E.

a range of wavenumbers between $k \sim 3 \times 10^{-3}$ and 10^{-2} km^{-1} (100 to 300 km). The upper portion of this wavenumber range has a KE spectral slope of -3 in the simulations (Fig. 3b). There is little indication of a $-5/3$ range in any of the cases although the model geometry may not be adequately large to allow this to develop. The spectra at smaller scales tend to fall off more rapidly as one reaches the dissipation scales in the model. The latter scale is estimated as the place in the kinetic energy spectra where the Reynolds number becomes one, *i.e.*

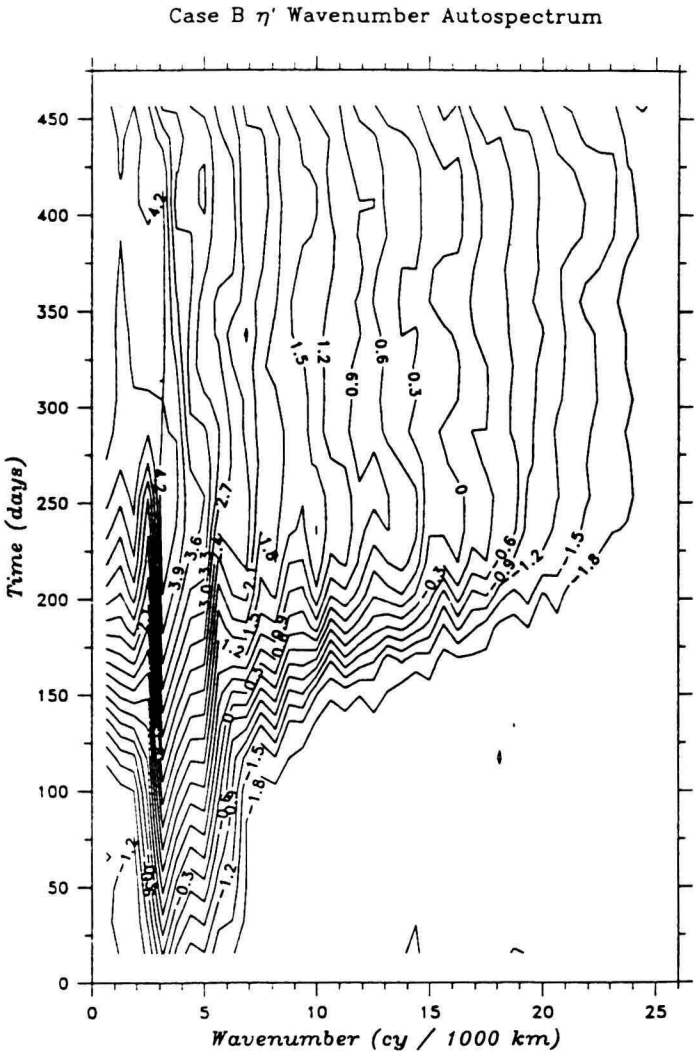

Fig. 4. Spectra evolution for sea surface height for case B as a function of time. The plot is constructed from individual spectra calculated at 15 day time intervals. The base-10 logarithm of the spectral density is contoured. For a discussion of the major time periods in the evolution of the turbulent spectra see the text.

$R_E = UL^2/K_H = 1$. From the kinetic energy spectra in the simulations and $K_H = 100\ m^2/s$ the dissipation range corresponds to wavenumbers $k \sim 2x10^{-1}\ km^{-1}$ or $L \sim 30$ km. The overall Reynolds number in these simulations exceeds 3000.

The evolution of the spectrum over time for case B is shown in Fig. 4. The less unstable case (D) has a more wave-like structure throughout the model run as compared to the more unstable cases (A,B). All of the unstable cases eventually evolve into similar near-equilibrium states although the transition to this state occurs at different times (Fig. 5). The near-neutral (E) and stable cases (F) also equilibrate but with very different final states as noted above.

The initial hundred days of each run is dominated by slow energy transfers associated with the linear growth phase and the initial onset of nonlinear but inefficient wave-wave interaction processes (Figs. 4,5). The early periods as displayed in Figs. 4 and 5 essentially follow the linear growth curves expected from theory. This is followed by a sharp transition period which is relatively short (Fig. 4) and involves peak energy transfers as shown for cases A, B and C in Fig. 5. These energy transformations involve large transfers of mean potential energy to the eddy field and the creation of significant new mean kinetic energy in the form of jets which will be discussed in more detail below. This transition period is followed by a long quasi-equilibrium period where the spectra are of nearly constant form (Fig. 4). The energetics in this final equilibrium period of cases A and C involve an end of the transition of eddy kinetic to mean flow energy and a more or less steady set of conversions of potential energy to both kinetic energy pools. Case B although it is fairly steady in spectral space is still very variable in terms of energy transformations (Fig. 5). The potential vorticity fields for cases A and B for three periods spanning transition are shown in Fig. 6.

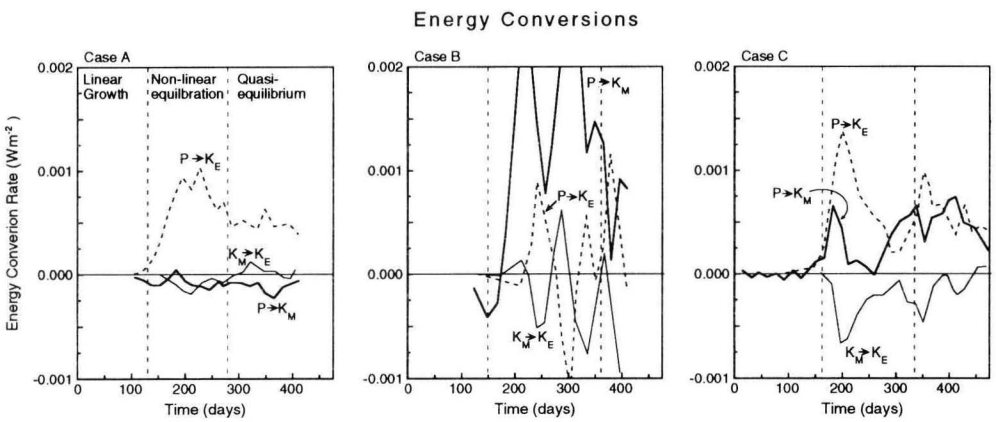

Fig. 5. Energy conversions for cases A, B, and C showing the energetics of the major periods of development as in Fig. 4. The energy conversions include conversion of potential to mean ($P \rightarrow dK_M$) and eddy ($P \rightarrow dK_E$) kinetic energy and the conversion of mean to eddy kinetic energy ($K_M \rightarrow dK_E$). Note the differences between the three cases. The influence of β in stabilizing the energy conversions in time is evident for both case A and C (eastward shear across one interface) in contrast to the sharp oscillations in the $P \rightarrow dK_E$, $K_E \rightarrow dK_M$ conversions for case B (westward shear in across both interfaces). components in case B

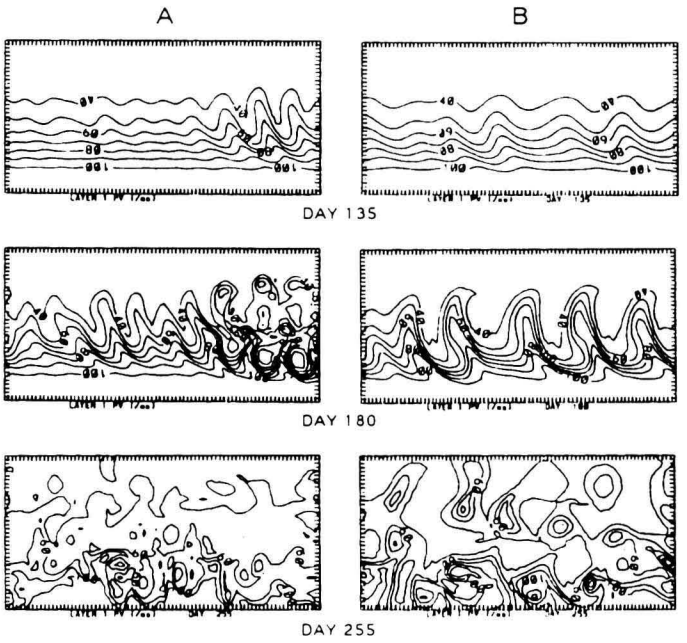

Fig. 6. Potential vorticity ($X\ 10^{-8}\ m^{-1}\ s^{-1}$) for the upper layer in the channel at three different times spanning the transition to turbulence for cases A and B. Note the inhomogeneity along channel in both cases at the end of initial phase of flow evolution (day 135). The transition is also very different between the short wave dominated cases (A,C) and B as obvious from the selected scales at days 180 and 255. It is the zones of concentrated potential vorticity gradient, when averaged along-channel, that correspond to the surface intensified frontal jets. In this sense there are not continuous jets but net mean flows made up of a series of jet streaks. The more homogeneous regions in the potential vorticity maps are the locations of the barotropic mean zonal flows.

Transition to turbulence and the quasi-equilibrium states

The transition period in Fig. 5 is associated with a strong transfer of energy back into zonal mean flows in the channel from the eddy field and peak transformations between potential and eddy kinetic energy. Similar transitions are observed in all of the unstable cases. As noted above, the nature of these transfers varies with position in the stability space. While the different cases (A,B,C,D) all reach similar spectral forms, the route to turbulence and the energy partition between potential and kinetic in the final eddy field differs substantially. In the cases dominated by short wavelengths (A, C, D; Fig. 2; Halliwell *et al.*, 1994), coherent eddies that appear at the time of transition are near the radius of deformation. These features emerge from the flow in a localized region of the channel in case A and then slowly expand to fill the channel through interaction with a set of fronts that are produced along the channel front at the time of transition (Fig. 6). While these fronts are not continuous features they show up as velocity

jets in the along channel mean flow. The final eddy field in case A is very barotropic with a KE to PE ratio of five. Case B has slightly longer wavelengths in the initial eddy field (Fig. 2) and represents a westward flow in both of the upper layers that is not stabilized by beta. Even though the linear growth rate for B is less than either A or C, it enters the nonlinear equilibration stage (Fig. 5) at approximately the same time and the energetic conversions during this phase are considerably more intense. Case B does not settle down to a steady set of energy conversions even though the spectrum reaches a constant form suggesting a steady state cascade range that began well before the dashed line in Fig. 5. Transition in case B is marked by the breaking of a train of waves as opposed to the coherent eddy formation process in case A (Fig. 6). Case B is even more barotropic (KE to PE ratio of 7) and again has along channel fronts which lead to channel average zonal jets (Fig. 6, day 255). The other cases (not shown) are less barotropic in the eddy field and have transitions which are a mixture between the case A and B extremes in the character of transition with respect to waves versus coherent features.

The spectral character of the final states has already been shown in Fig. 3. There are several questions about these states and the manner in which they are reached that deserve further comment. First of all, how is the energy partitioned and does the scaling suggested by Fu (1983) actually work? Calculations of the kinetic energy spectra (Fig. 3b for cases A and E) as compared with the potential energy spectra agree with that predicted by the k^{-2} PE scaling hypothesized by Fu (1983) in the case A, B, C and D model runs. The neutral and stable cases (E,F) do not obey this scaling and have kinetic energy spectra that are steeper than their η spectra. The isolated peaks in these spectra suggest dominant wave numbers tied to a combination of initial conditions and the initial perturbation structure. The suggestion is that there is not a well developed inertial range in these cases. The model spectra bound those observed in the altimeter data. In fact the full set of observed spectra along GEOSAT altimeter tracklines falls exactly between -2 and -5. The ten degree averaged spectra in Fig. 1 have a more truncated wavenumber range due to the band averaging performed.

Conclusions

This is a preliminary report on attempts to understand the nature of the ocean eddy field based on analytical stability space analysis and long spin-down mode simulations with a compatible primitive equation model. The results compared to the available observations of the ocean interior are promising in the sense that the resulting spectra bound those observed from satellite altimeters. The nature of turbulence in the locally stable domains which correspond to the low spectra fall-offs in the observations demand more work to determine to what extent the eddy variability is wind-forced or is either advected or propagated into the mid-gyre from distant unstable regions. The fact that unstable states, even in proximity to the stability boundaries in the linear problem, approach a

k^{-5} PE cascade range and a k^{-3} KE supports Fu's (1983) hypothesis. In addition all of the initial problem experiments approach Charney's (1973) case in terms of energy equi-partition and then exceed it in all unstable cases except D with the KE dominating the PE by factors of up to seven in case B. This suggests very barotropic final states for the eddy field in the very unstable cases (A, B, and C). All of the highly turbulent cases produce pronounced zonal mean flows in the channel. These intense zonal flows are marked with surface intensified jets embedded in more barotropic flows. The creation of rectified flows has long been appreciated in turbulence theory (Starr, 1968; Vallis and Maltrud, 1993) although their role in governing the transition to turbulence and the dynamics of turbulent cascades is still an important area of investigation.

The simulations presented here are preliminary and need to be followed up with a further exploration of parameter space. A set of simulations cutting across the linear stability space are currently underway. An even more relevant issue would be to consider the forced equilibrium states that can reach true equilibrium. While means of doing this without full ocean basin simulations is currently being considered, it is not simple to design such calculations.

Acknowledgements

The authors would like to thank Kevin Leaman for help with the GEOSAT spectra and the remote sensing group for basic data processing. Annalisa Griffa for constructive comments on the discussion of the turbulence theory. This research is funded by the Office of Naval Research (N00014-89-J1536, DO and GP), the National Aeronautics and Space Administration (NASA NGT-30026, CF) and the National Science Foundation (NSF OCE-9206643).

References

Andrews, D.G. and B.J. Hoskins, 1978 - Energy spectra predicted by semi-geostrophic theories of frontogenesis, *J. Atmos. Sci.* **35**, 509–512.

Bleck, R and D. Boudra, 1986 - Wind-driven spin-up in eddy- resolving ocean models formulated in isobaric and isopycnic coordinates. *J. Geophys. Res.* **91**, 7611–7621.

Boudra, D., R. Bleck and F. Schott, 1988 - A numerical model of instabilities in the Florida current. *J. Mar. Res.* **46**, 715–751.

Charney, J.G., 1971 - Geostrophic turbulence, *J. Atmos. Sci.* **28**, 1087–1095.

Charney, J.G., 1973 - Planetary Fluid Dynamics, In: *Dynamic Meteorology*, P. Morel, ed., D. Reidel, Dordrecht, 97–351.

Cushman-Roisin, B., G.S. Sutyrin, and B. Tang, 1992 - Two-layer geostrophic dynamics. Part I: Governing equations. *J. Phys. Oceanogr.* **22**, 117–127.

Dantzler, H.L., 1976 - Geographic variations in the intensity of the North Atlantic and North Pacific oceanic eddy fields. *Deep – Sea Res.* **23**(9), 783–794.

Davey, M.K., 1977 - Baroclinic instability in a fluid with three layers. *J. Atmos. Sci.* **34**, 1224–1234.

Denman, K. and T. Platt, 1976 - The variance spectrum of phytoplankton in a turbulent ocean. *J. Mar. Res.* **34**, 593–601.

Forbes, C., K.D. Leaman, D.B. Olson and O. Brown, 1993 - Eddy and wave dynamics in the South Atlantic as diagnosed from GEOSAT altimeter data. *J. Geophys. Res.* **98**, 12,297–12,314.

Fu, L.L., 1983 - On the wave number spectrum of oceanic mesoscale variability observed by SEASAT altimeter. *J. Geophys. Res.* **88**, 4331–4341.

Gower, J.F.R., K.L. Denman, and R.J. Holyer, 1980 - Phytoplankton patchiness indicates the fluctuations spectrum of mesoscale oceanic structure. *Nature* **318**, 157–159.

Halliwell, Jr., G.R., G. Peng, and D.B. Olson, 1994 - Stability of the Sargasso Sea subtropical frontal zone. *J. Phys. Oceanogr.* **24**, 1166-1183.

Hua, B.L. and D.B. Haidvogel, 1986 - Numerical simulations of the vertical structure of quasi-geostrophic turbulence. *J. Atmos. Sci.* **43**, 2923–2936.

Kolmogoroff, A.N., 1941 - The local structure of turbulence in incompressible viscous fluid for very large Reynolds numbers. from *Comptes Rendus (Doklady) de l'Academie des Sciences de l' U.R.S.S.* **30**, 301–305.

Kraichnan, R.H., 1967 - Inertial ranges in two-dimensional turbulence. *Phys. Fluids* **10**, 1417–1423.

Le Traon, P.Y., M.C. Rouquet, and C. Boisser, 1990 - Spatial scales of mesoscale variability in the North Atlantic as deduced from GEOSAT data. *J. Geophys. Res.* **95**, 20,267–20,285.

Nof, D., 1981 - On the beta-induced movement of isolated baroclinic eddies. *J. Phys. Oceanogr.* **11**, 1662–72.

Olson, D.B., 1991 - Rings in the ocean. *Ann. Rev. Earth and Planetary Sciences* **19**, 283–311.

Pedlosky, J., 1979 - *Geophysical Fluid Dynamics*. Springer-Verlag, New York, New York, 710 pp.

Phillips, O.M., 1971 - On spectra measured in an undulating layered medium. *J. Phys. Oceanogr.* **1**, 1–6.

Rhines, P.B., 1975 - Waves and turbulence on a beta plane. *J. Fluid Mech.* **69**, 417–443.

Rhines, P.B., 1977 - The dynamics of unsteady currents. In *The Sea*, edited by E. D. Goldberg *et al.* **6**, Wiley Interscience, New York, 189–318.

Salmon, R., 1982 - Geostrophic Turbulence. In *Topics in Ocean Physics*, Soc. Italinana di Fiscia, Bologna, 30–78.

Starr, V.P., 1968 - *Physics of Negative Viscosity Phenomena*. McGraw-Hill, New York, 256 pp.

Tang, B. and B. Cushman-Roisin, 1992 - Two-layer geostrophic dynamics. Part II, Geostrophic turbulence. *J. Phys. Oceanogr.* **22**, 128–138.

Vallis, G.K., 1992 - Problems and phenomenology in two-dimensional turbulence. In: *Nonlinear Phenomena in Atmospheric and Oceanic Sciences* G.F. Carnevale and R.T. Pierrehumbert, Eds., Springer-Verlag, New York, 1–25.
Vallis, G.K. and M.E. Maltrud, 1993 - Generation of mean flows and jets on a beta plane and over topography. *J. Phys. Oceanogr.* **23**, 1346–1362.

Rosenstiel School of Marine and Atmospheric Sciences
University of Miami
4600 Rickenbacker Cswy.
Miami, FL 33149
USA